PCCP

PAPER

View Article Online
View Journal | View Issue



Cite this: *Phys. Chem. Chem. Phys.*, 2018, **20**, 28114

# Free-standing Pt and Pd nanowires: strain-modulated stability and magnetic and thermoelectric properties†

Shivam Kansara, [a] Sanjeev K. Gupta, *[b] Yogesh Sonvane *[a] and Ashok Kumar [c]

Received 25th July 2018,
Accepted 10th October 2018

DOI: 10.1039/c8cp04731f

rsc.li/pccp

We studied the Lagrangian strain-induced colossal magnetism and thermoelectric performance of platinum (Pt) and palladium (Pd) nanowires (NWs) using first-principles density functional calculations. Pt and Pd NWs were found to be dynamically stable for both strain-free and strained situations. Their cohesive energy and magnetic moment showed decrease and increase, respectively, with an increase in tensile Lagrangian strain (2% to 10%) in the (001) plane. Furthermore, we analyzed the thermodynamic properties using the quasi-harmonic approximation (QHA), heat capacity and internal energy of both NWs originating at 0 K, where their internal energy (*E*) remained high. For the NWs with the (100) and (010) planes, magnetism exist in the strain-free case, whereas it decreases rapidly on increasing the value of strain. Our results predict the excellent stability, colossal magnetism, and thermoelectric properties of the studied NWs; therefore, these NWs can be used as potential thermoelectric materials for device applications.



## 1. Introduction

Noble metal nanowires have attracted immense research interest owing to their potential technological applications.[1–3] Various experimental techniques such as scanning electron microscopy (SEM), atomic force microscopy (AFM), contact resonance AFM, nanoindentation, micro-electro-mechanical-system (MEMS)-based testing and mechanically controllable break junctions are available for the study and characterization of atomically thin nanowires. Several experimental[4] and theoretical[5–8] studies have been devoted to investigate the properties of metallic nanowires including Hf, W, Co, Fe, Pt, and Au nanowires. Atomic chains of Au are short suspended monatomic wires, which are primarily synthesized and imaged *via* transmission electron microscopy (TEM)[9,10] and the conductance is characterized by break junction experiments.[11–13] Similarly, suspended Pt and Pd monoatomic nanowires were also synthesized.[14–16]

The magnetic properties of transition group systems should be dealt with at the atomic level, which can be analyzed using the electronic structure of the systems. It is known through theoretical analysis that one-dimensional atomic arrays may not be ferromagnetic in all cases. Also, surfaces, clusters and nanowires offer templates to study magnetic anisotropy.[17,18] Orbital moments are emphatically eliminated by crystal fields; thus, the value of anisotropy is very small in the case of bulk counterparts.[19,20] In the past, experimental and theoretical studies have been focused on nanoelectronic magnetic devices with spin-polarized electron transport in various one-dimensional (1D) nanostructures.[20–22] Chopra *et al.*[23] established the relationship between magnetic and transport properties of magnetic nanocontacts by giving the name "giant magnetoresistance" (GMR).

There are many ways to explore the electronic, magnetic, thermal and optical properties of 1D materials for desired applications;[24–33] however, mechanical strain engineering has been proven to be one of the efficient techniques. Also, tuning the diameter of NWs, such as Pd and Pt NWs, can effectively lead to applications in free-standing membranes, which results in excellent electro-catalytic movement,[34] high-performance hydrogen sensors,[35,36] oxygen reduction responses,[30] highly efficient fuel-cell catalysts[37] and electrochemical amperometric biosensors.[38] Pt NWs exhibit magnetic moment, which is ascribed to the extension of interatomic bonding in Pt atoms.[39] In previous experiments, researchers successfully synthesized ultrathin Pt nanowires up to 300 nm, which spontaneously self-assembled into bundles without the utilization of any stabilizer and any external field.[37,40] Recently, various vdW-corrections,

[a] *Advanced Materials Lab, Department of Applied Physics, S.V. National Institute of Technology, Surat 395007, India. E-mail: yas@phy.svnit.ac.in*
[b] *Computational Materials and Nanoscience Group, Department of Physics, St. Xavier's College, Ahmedabad 380009, India. E-mail: sanjeev.gupta@sxca.edu.in*
[c] *Department of Physical Sciences, School of Basic and Applied Sciences, Central University of Punjab, Bathinda, Punjab 151001, India*

† Electronic supplementary information (ESI) available. See DOI: 10.1039/c8cp04731f

 

*i.e.*, DFT-D2 and DFT-D3 and XC functionals, *i.e.*, LDA and GGA have been used to show the effect of tensile and compressive strengths in bulk metals such as coinage metals and transition metals using representative DFT methods.[41,42] These long range corrections are dedicated to finding weak interlayer bonding properties of low-dimensional materials for affording accurate bonding descriptions, *i.e.*, conjugated π–π molecular systems, which were recently revealed in two-dimensional (2D) systems.[43–45] VdW interactions ensure that the fundamental properties of systems such as size (lattice constant) and cohesion energy are not neglected. For a solid covalently bonded structure, dispersion interactions play a significant role in the static properties. However, vdW-correction DFT-D2 gives extremely inconsistent and qualitatively inappropriate outcomes for the tensile strength of bulk Pd.[42,46] The real conductance of an atomic wire depends on precise orbital coverage, that is, the bond between the atoms or even the wire length.

In this study, we examined the phonon spectra, magnetic properties and thermoelectric performance of strained (0% to 10%) Pd and Pt NWs. The discussed NWs have attracted much attention due to their real-life applications in nanoscale devices. This inspired us to focus on the impacts of strain on the magnetic and cohesive properties, anisotropy and stress in NWs. This paper is organized as follows: Methodology and computational details are presented in division 2, followed by Results and discussion in division 3, and Conclusions are discussed in division 4.

## 2. Methodology

Spin-polarized density functional theory (DFT)[47] calculations were performed using the Quantum ESPRESSO (QE) package.[48] Vanderbilt ultrasoft pseudopotentials[49] were used to treat electron–ion interactions. The exchange–correlation term was defined using the generalized gradient approximation (GGA) within the Perdew–Wang (PW91) parameterization,[50] and hybrid HSE06[51,52] functional. A vacuum space of 15 Å along $x$ and $y$ directions with the lattice parameters of $a$ and $b$ were taken to avoid the interactions between the periodic replicas. Atomic positions were fully relaxed until the Hellman–Feynman forces on each atom became less than 0.02 eV Å$^{-1}$. We utilized a plane-wave basis set with the kinetic energy cutoff of 700 eV. The self-consistent convergence of energies was taken as $10^{-10}$ eV atom$^{-1}$. A Monkhorst–Pack of $2 \times 2 \times 40$ $k$-points was used for the self-consistent field sampling, whereas for the non-self-consistent field, it was $2 \times 2 \times 50$ at gamma-centered calculations.

The magnetic anisotropy was correlated to quenching/dequenching of the orbital moment based on the spin direction. The magnetic moment ($\mu_B$) of the nanowire is given as (1):

$$M = i\sum_{j\sigma}^{\text{occ}} \int \left[\Psi_j^{\sigma}(r)\right]^{*} \frac{\partial \Psi_j^{\sigma}(r)}{\partial \phi} \mathrm{d}^3 r \qquad (1)$$

Here, $\psi_j^{\sigma}$ and $\phi$ are the two-component spinor wave functions and the angle around the wire axis, respectively, and the sum runs over the occupied states in the atomic core regions of the ultrasoft pseudo-potentials.

To understand the thermodynamic properties, the first step was to inspect the lattice vibrational modes (phonons) of the material. The number of atoms, $N = 3$, in the primitive cell led to three acoustical (A) and six $(3N - 3)$ optical (O) phonon modes. The displacement of the atoms along the $x$-direction was equivalent to a displacement along the $y$- or $z$-direction. Heat capacity, where all the oscillators in a solid are harmonic and have fixed frequencies, can be derived from Planck's distribution. The heat capacity at a constant volume, $C_V$, for the mode i is[53]

$$C_V(T) = k_B \left(\frac{\varepsilon_i}{k_B T}\right)^2 \frac{\exp(\varepsilon_i/k_B T)}{\exp(\varepsilon_i/k_B T - 1)^2} \qquad (2)$$

where $k_B$ and $T$ are the Boltzmann constant and temperature in K, respectively. Thermoelectric properties (thermal and electrical conductivity) were calculated using the semi-classical Boltzmann theory, as executed in the BoltzTrap code.[54]

## 3. Results and discussions

### A. Structural analysis

NWs were modeled from alternate stacks of (110) atomic planes of FCC, where two atoms were taken from each plane and one atom was center to the cell to model a NW along ⟨110⟩. Thus, the atoms from each plane seemed to form a dimer. The NWs were adjusted along the $z$-axis and demonstrated utilizing tetragonal supercells, as shown in Fig. 1(a and b). The interatomic spacing associated with the calculated zero-strain interatomic spacing ($d$) and angle $\theta$ (°) ranged from 2.74 Å to 2.72 Å and 83° to 85°, respectively. The equilibrium lattice constants to the $z$-direction for lattice parameter $c$ were calculated to be 2.57 Å and 2.61 Å for Pd and Pt NWs, respectively. Previously, the tetragonal phases of Pd and Pt metals and their alloys were discussed.[55–60] When strain is applied to the system, all atoms are allowed free motion. Thus, an optimized equilibrium position for all atoms of the twisted unit cell was used in the calculation, which yields the minimum total energy for the forced strain condition of the supercell. First, we considered Lagrangian strain ranging from 2% to 10% with an increment of 2% along the $z$-direction. The strain-stress curve (Fig. 1c) reveals that the tensile strength of Pt NWs is almost double that of Pd NWs. Also, cohesive energy of both NWs decreases monotonically on increasing the value of strain (Fig. 1d). The cohesive energy ($E_{\text{cohesive}}$) is calculated as follows:

$$E_{\text{cohesive}} = \frac{\left(E_{\text{complex}} - nE_{\text{atoms}}\right)}{n} \qquad (3)$$

Here, $E_{\text{complex}}$ and $E_{\text{atoms}}$ are the total energy of the complex system and energy of a free atom, respectively, and $n$ is the number of atoms in NWs. The values of the lattice constant (LC), nearest distance ($d$), angle ($\theta$°) and magnetic moment along the (100) and (010) directions for different tensile Lagrangian strains (0% to 10%) are listed in Table S1 (ESI†). We calculated the

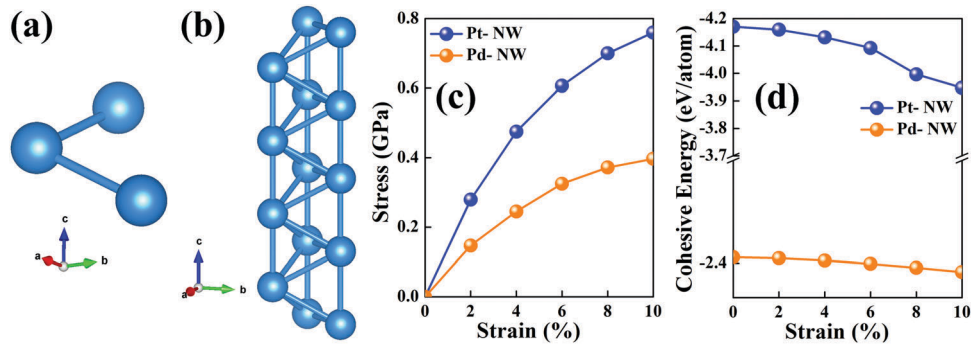


Fig. 1 Representative structures of the (a) side and (b) top views of the structure of NWs. (c) Stress–strain curves and (d) strain *versus* cohesive energy curves for Pt and Pd NWs.

magnetic moments for different diameters varying from ~3.30 Å to ~8.67 Å and found nonmagnetic behaviors of both NWs. The structures with different diameters of NWs are shown in Fig. S1 (ESI†).

Fig. 2 and 3 depict the phonon dispersion curves of Pt and Pd NWs, respectively. The nine phonon bands with three acoustical branches (LA, TA, and ZA) correspond to three atom/unit cell in Pt and Pd NWs. Out of these, six phonon bands form optical branches. All the acoustical branches exhibit linear dependence on frequency in the wave vector, implying a wavelength-independent speed for that mode, *i.e.*, NWs may carry a dispersionless medium for that mode. The other acoustical branches need a higher velocity for long wavelengths. The low-lying acoustical modes are absent in the spectra of both NWs, which show that Pt and Pd NWs are structurally stable materials. We noted that the maximum phonon frequency for Pd NWs is slightly larger than that of Pt NWs. Thus, these features of phonon dispersion may provide insights into the thermoelectric properties of given nanowires.[61] Usually, an increase in volume will weaken the bonding nature. Also, as strain is applied, the higher frequency band lines shift toward a lower frequency. With the application of 8% strain, the geometry of NWs is quite different from that of other samples. This case can be matched with strain-free NWs with three bands at low frequency.

In Pt NWs, all the phonon modes began with linear dispersion at a smaller strain; however, the out-of-plane mode did not change much with frequency and instead showed softening of the modes. It is also clear from the Fig. 2 that the splitting of the original degenerated modes of Pt NWs did not break their stability up to the applied 10% tensile strain and exhibited a real positive frequency for all the applied strains except 4% strain. Furthermore, there was no dramatic change in the nature of the phonon modes. Meanwhile, in the case of Pd NWs, the phonon

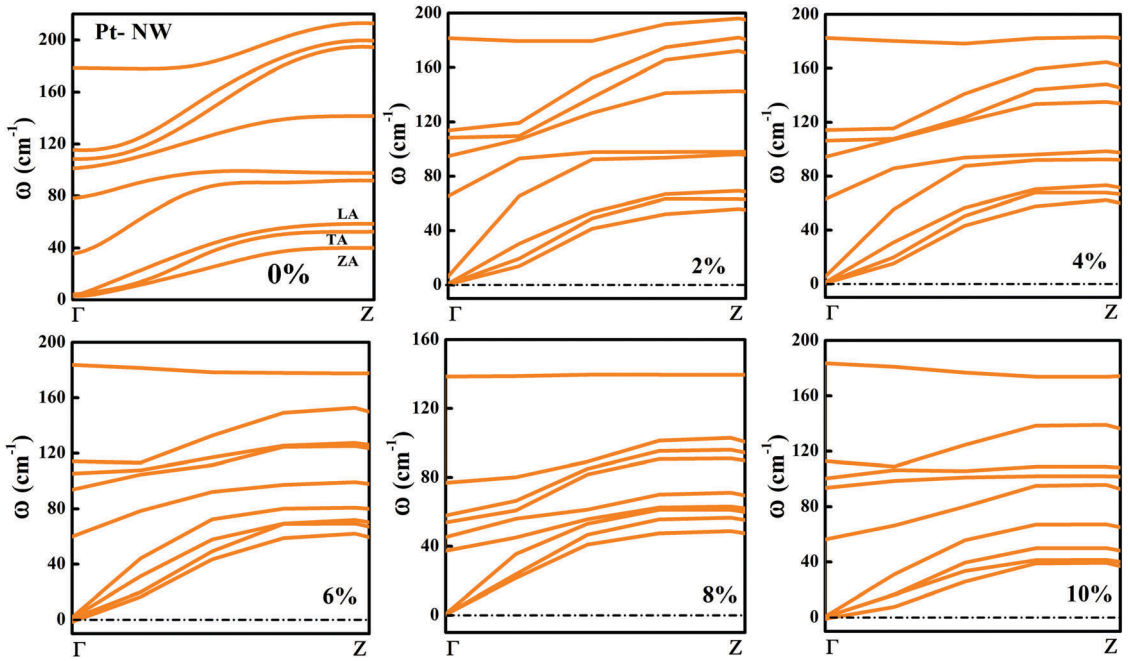


Fig. 2 Phonon dispersion curves of Pt NWs for 0% to 10% strain.

 

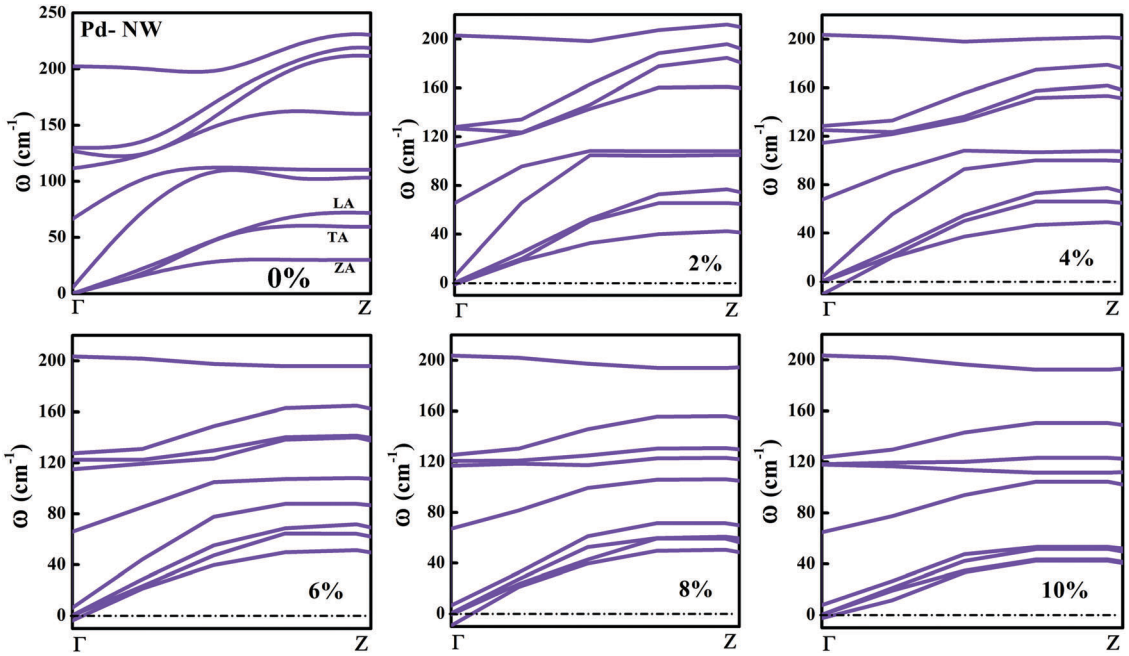


Fig. 3 Phonon dispersion curves of Pd NWs for 0% to 10% strain.

band structure showed a significant change in dispersion with the effect of strain. The strain-free Pd NWs were dynamically stable with real positive frequencies, whereas the out-of-plane mode (ZA) for strained NWs showed a small imaginary frequency at $\geq$4% applied strain. With an increase in the volume of NWs, the bonding and angles of their atoms changed. In the case of 4% and 8% strains, the geometries were different after optimization compared to those of others. Also, the instability conditions and mechanism of the systems under ideal tensile strengths and critical strains were confirmed.[62,63]

The phonon density of states (PDOS) for strain-free NWs approached to 0 as the frequency $\rightarrow$ 0, whereas strained Pd NWs showed finite PDOS in a few values of strain (Fig. S1, ESI†). The curvature of the phonon DOS showed different behaviors due to the weak and high range frequency. In PDOS, the lowest frequency part ($\sim$30–35 $cm^{-1}$) indicated very weak electron acoustic phonon coupling. From the phonon dispersion curves in Fig. 2 and 3, the phonon band gaps of Pt NWs appeared around 150 $cm^{-1}$, which indicated the application of highly stressed nanowires. In addition, the specific heat and internal energy of both NWs using quasi-harmonic approximation (QHA) are shown in Fig. S2 (ESI†) as T1 and related discussion on thermodynamic properties are given in the ESI† as T1. It was found that Pt NWs are more sustainable than Pd NWs under strain-free conditions.

### B. Strain effect on electronic and magnetic properties

The electronic band structure and density of states (DOS) of the studied NWs are given in Fig. 4. The bands crossing the Fermi levels mainly consist of d-states. From the electronic DOS, it is predictable that NWs are stable owing to the high energy and low density of the d-orbital at the Fermi level.[34] Looking at the electronic structure of NWs, the 5d and 6s states give 16 spin orbital bands for Pt NWs (Fig. 4). In both NWs, the large splitting of up and down spin DOS results in the existence of a magnetic moment for NWs. Insights into the bonding character of NWs were derived from the electronic charge density analysis. It is clear from Fig. 4(c–f) that along the atomic sphere, electrons are not limited, and their reasonable proportion resides in the interstitial region. Thus, the nature of the bonding is covalent for the strain-free systems. The strain-dependent electronic charge density is shown in Fig. S3 and S4 (ESI†) and electron charge transfer using Bader charge analysis is shown in Table S2 (ESI†). The charge density thermos can be used to distinguish the charge conductivity across the system. Next, we calculated the magnetic moment of all three deformation modes. It is important to note that tensile strain changes the atomic structure of NWs.[64] The unexpected anisotropic colossal magnetic moments ($\mu_B$) for the strain-free wire were calculated to be 2.16 $\mu_B$ (100-plane) and 0.83 $\mu_B$ (010-plane) for Pt and Pd NWs, respectively, which decreases with an increase in tensile strain. The spin magnetic moment mainly depends on the interatomic spacing and angle, which ranged from 2.68 Å to 2.74 Å and 83° to 91°, respectively, for NWs. Our calculated colossal magnetic moments were 1.48 $\mu_B$ and 1.30 $\mu_B$ for $d$ = 2.87 Å and 2.83 Å, respectively, for both Pt and Pd NWs.

Fig. 5 represents the conceptual diagram for electron transition under Lagrangian strain in the absence and presence of an external field. Here, half of the electrons have spin in $z$-directions and remaining electrons have a negative spin direction in the absence of an external field; thus, the resultant net magnetization is zero. On applying Lagrangian strain along the $z$-direction, the parallel spins along $B$ went down by $\mu_B B$, whereas in the opposite direction to $B$, the spins went up. This situation is

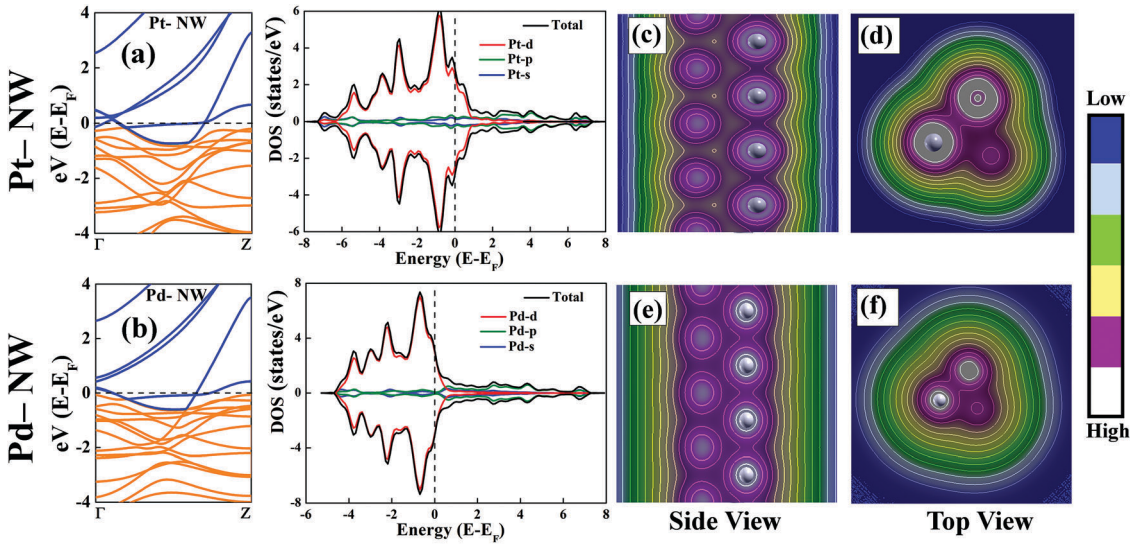


Fig. 4 (a and b) Electronic band structure and spin-polarized partial density of states of Pd and Pt NWs. Orange color represents the valence bands and blue color represents the conduction bands. (c and e) (Side view) and (d and f) (top view) of the electron charge density of Pt and Pd NWs. The side color bar shows the electron charge density scale (electrons per Å$^3$). The blue and grey colors show minimum and maximum charge densities, respectively, and the isolines indicate the equipotential surface.

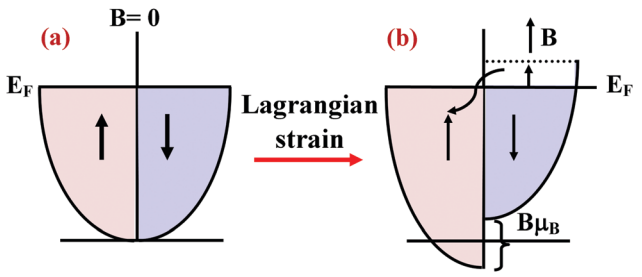


Fig. 5 Concept diagram for (a) when $B$ = 0, the Fermi–Dirac distributions are equal and thus, $M$ = 0; (b) when Lagrangian strain is applied, all the anti-parallel spins change to parallel spins.

dynamically unstable; hence, the electrons near the Fermi level jumped from the antiparallel half spin to the parallel spin and net magnetization started to occur. The one-dimensional Bloch functions are eigenstates of the $z$-components of total angular momentum ($j$) and half integer eigenvalues of the split magnetic states $m_j$.[65] The matrix elements of spin matrices can be given as follows:

$$\left\langle \mathrm{p}_{5/2}|\sigma_\alpha|\mathrm{p}_{5/2}{}'\right\rangle = \mathrm{p}\delta_{\mathrm{pp}'}\delta_{\alpha z} \quad (4)$$

Here, p, p′ can be positive or negative and $\sigma_\alpha$ as $\alpha = x, y, z$ are the Pauli matrices in the spin–orbit limit.

It was found that the population of the anti-bonding states at the Fermi level (Fig. 6) is responsible for the electronic instability that leads to spin contamination, which plays an important role in shifting the energy level of NWs. Ferromagnetism appeared after the removal of these anti-bonding states from the Fermi level. The d-states exhibited splitting under an external field due to the spin sub lattices and rearrangement of charge density. The magnetism or polarization effects in NWs have been described in Fig. 7. Spin polarization is a default property of materials but here, it arises due to the strain in both NWs. The mechanism of the origin of magnetism due to splitting of d states as α- and β-spin contamination was proposed by Stoner.[66,67] Briefly, Stoner introduced I·DOS ($\varepsilon_F$) > 1, where I and DOS ($\varepsilon_F$) are the strength of the exchange interaction of the metal system and density of state at the Fermi level, respectively. Also, in NWs, each atom is bonded with two neighboring atoms; thus, the magnetic moment strongly depends on the distance of the neighboring atoms. As shown in Fig. 7, the magnetic moment and polarization values increased with increasing strain, which led to an increase in the colossal magnetic moment of NWs, for which symmetricity is responsible.

To understand the reason for magnetism, we examined spin polarization of the electrons and magnetic moment of Pd and Pt NWs. From projected density of states (PDOS), we can understand the magnetic moment and polarization by orbital contribution. The proportion of density of states up spin ($D_{\mathrm{up}}$) and down spin ($D_{\mathrm{down}}$) electrons at the Fermi level is spin polarization. This can be determined using eqn (5):[68–70]

$$P = \frac{(D_{\mathrm{up}} - D_{\mathrm{down}})}{(D_{\mathrm{up}} + D_{\mathrm{down}})} \quad (5)$$

In Fig. 4, Pt and Pd NWs showed zero spin polarization, which confirms their non-magnetic behavior.[71–73] The quantum confinement may be the reason for the zero spin polarization shown in Fig. 4. Fig. 6 shows ferromagnetic behavior with negative spin polarization, where the electrons with down spin dominate the Fermi region.

To determine the anisotropy magnetic moment, we performed calculations for all three deformation modes, where it is important to consider tensile strain because the properties are believed to change in the atomic structure with only tensile strain. Thus,

 

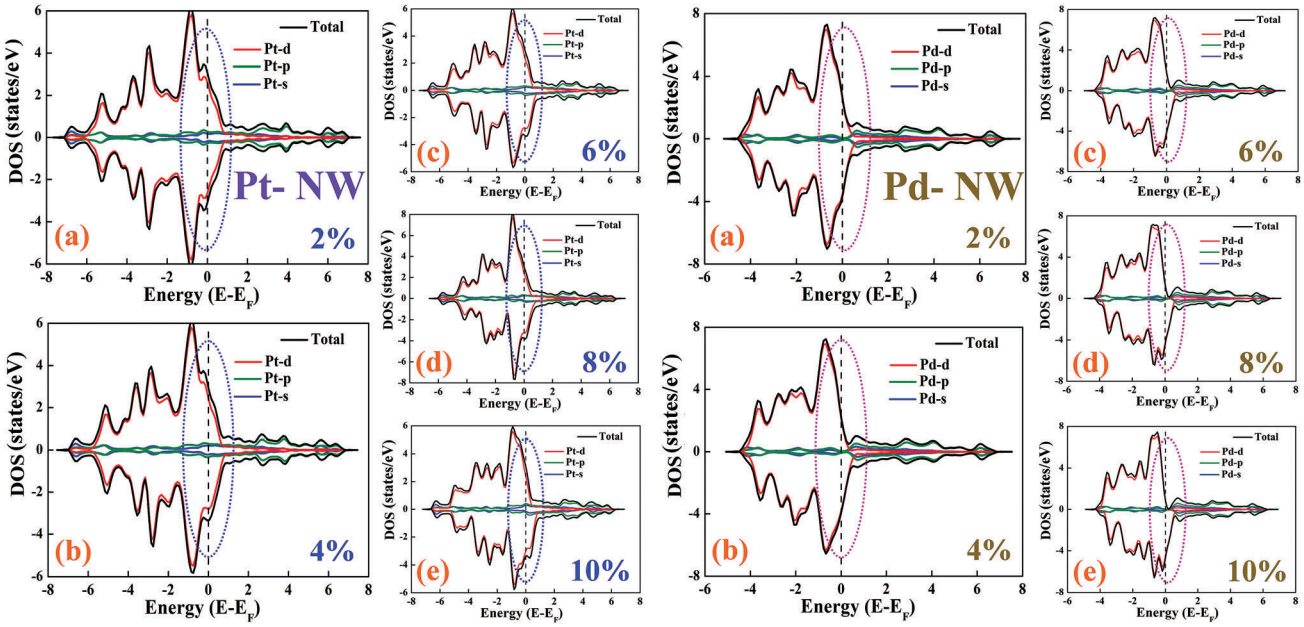


Fig. 6 Projected density of states (PDOS) represented with spin up and spin down channels for both NWs at different Lagrangian strains. The circle around the Fermi level shows the changes in spin upon the application of strain.

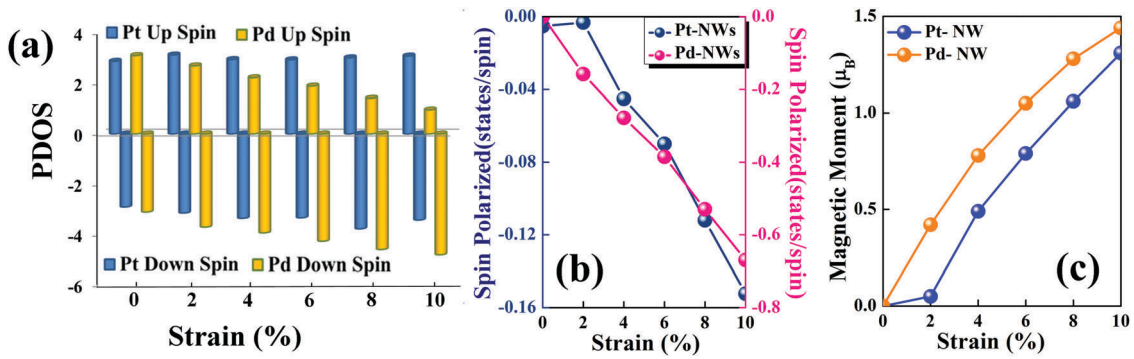


Fig. 7 Values for up spin, down spin, spin polarization and magnetic moment for Pt and Pd NWs at different tensile Lagrangian strains.

it should be noted that the unexpected anisotropy colossal magnetic moments ($\mu_B$) at free-strain were 2.16 ($\mu_B$) (100-plane) and 0.83 ($\mu_B$) (010-plane) for both cases, which decreased with respect to an increase in tensile strain. The anisotropy in the magnetic moment was also reported in previous studies.[15,61,74–77] For example, the magnetic moments for Pt NWs were calculated to be 0.90 $\mu_B$ and 0.80 $\mu_B$ for parallel and perpendicular to the wire,[74] respectively, whereas the values were 0.47 $\mu_B$ for central, 0.81 $\mu_B$ for infinite, and 0.56 $\mu_B$ for parallel NWs.[15] Similarly, the magnetic moment for Pd NWs varied with an increase in their length.[76–80] The magnetic moments of the respective NWs were also calculated using the HSE06 hybrid functional, which are presented in the ESI† as Fig. S4. The values of the magnetic moments of PBE and HSE06 were very close to each other.

### C. Thermoelectric properties

The electron relaxation time, $\tau_e$, is a necessary parameter for the calculation of thermoelectric properties. In the BoltzTrap code, the semi-classical transport coefficient is treated, and it is based on a smoothened Fourier interpolation of the bands. Here, $\tau_e$ varied with strain, carrier concentration and temperature, and we only considered the effect of temperature on the electron relaxation time $\tau_e$. The standard electron–phonon dependence for $\tau_e$ is $\tau_e = CT^{-1}n^{-1/3}$, where $C$ is a constant and $T$ is temperature in K. The phonon-boundary scattering was considered with the Debye–Callaway model, which is frequency- and temperature-independent. Thus, the thermal conductivity basically follows $T^3$. As temperature increased, the thermal conductivity increased due to impurity and phonon–phonon scattering.

The results demonstrate excellent electronic thermal and electrical conductivities of Pd and Pt NWs (Fig. 8). The thermal (electrical) conductivity values of Pt and Pd were 91 W m$^{-1}$ K$^{-1}$ ($4.70 \times 10^7$ S m$^{-1}$) and 70 W m$^{-1}$ K$^{-1}$ ($3.77 \times 10^7$ S m$^{-1}$), respectively, at 800 K. Bhatta *et al.*[81] reported the thermal conductivity values of Pt NWs in previous studies, which were 80 W m$^{-1}$ K$^{-1}$ and 90 W m$^{-1}$ K$^{-1}$ at 700 K and 800 K. Similarly,

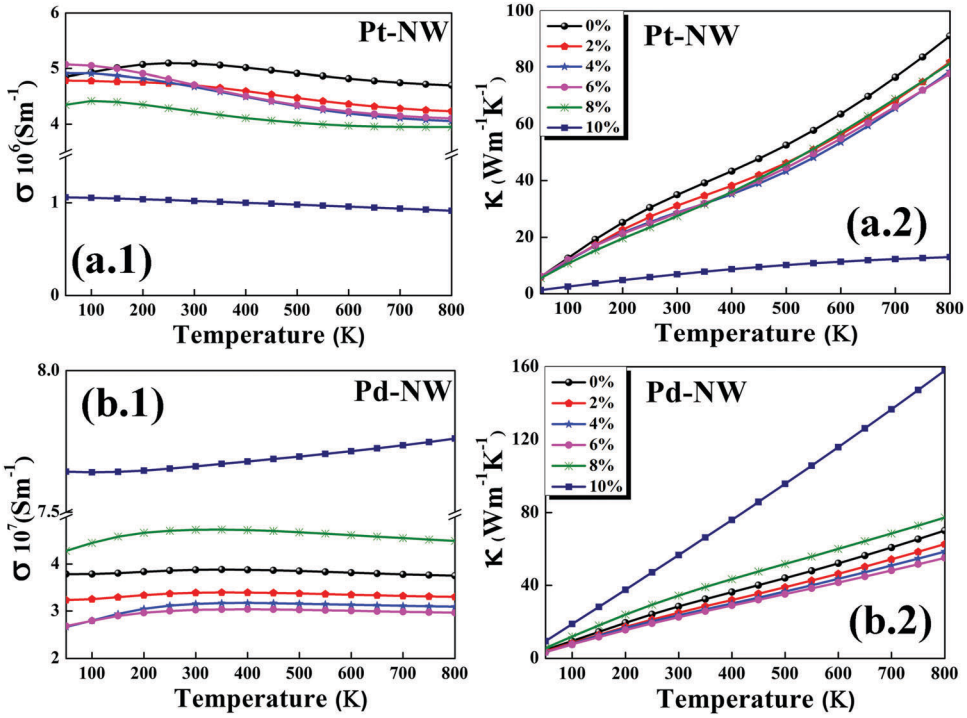


Fig. 8 (a.1) and (b.1) Electrical conductivity and (a.2) and (b.2) electronic thermal conductivity of Pt and Pd NWs as a function of temperature.

Terada *et al.*[82] reported the thermal conductivity of a Pt monoatomic wire to be 95 W $m^{-1}$ $K^{-1}$ at 1100 K. The electrical conductivity of Pt was 2.15 × $10^6$ S $m^{-1}$ for wire and 9.5 × $10^6$ S $m^{-1}$ for bulk.[83] In the case of Pd, the thermal conductivity value of 85.3 W $m^{-1}$ $K^{-1}$ was found at the onset of melting, whereas at the beginning of the liquid phase, it was calculated to be 54 W $m^{-1}$ $K^{-1}$.[84] Zinovyev *et al.*[85] reported a value of 86 W $m^{-1}$ $K^{-1}$ at 1600 K. Vlasov *et al.*[86] reported thermal conductivity values at the end of the solid phase and the beginning of the liquid phase as 99 and 87 W $m^{-1}$ $K^{-1}$, respectively. The electrical conductivity values of 3.0 × $10^7$ S $m^{-1}$ at 300 K[87] and 0.95 × $10^7$ S $m^{-1}$ at 1740 K[88] were reported for bulk Pd, whereas the value of 0.88 × $10^7$ S $m^{-1}$ was reported at 1740 K.[88] Thus, it can be concluded that our studied NWs have high thermal and electrical conductivities. The calculated thermoelectric properties such as electrical and thermal conductivity in Fig. 8 show conductivity at various strains, which can be useful for integrated devices under the desired pressure.

## 4. Conclusions

To date, there has been significant research on the use of Pt and Pd NWs for catalysis, biomedical and clean environment applications. However, very few studies have been reported the stability of NWs under strain and electric field with and without mechanical properties. We determined the structural, magnetic and vibrational properties of Pt and Pd NWs using first-principles calculations based on DFT. Increasing the tensile Lagrangian strain (2% to 10%) led to favorable conditions, which increased the colossal magnetic moment and decreased the cohesive strength of NWs in the (001) plane. The results showed that the magnetic moments of Pd NWs are larger than that of Pt NWs, whereas the cohesive energy of Pt NWs is higher than that of Pd NWs. Moreover, their stability was confirmed by the phonon dispersion curves for strain-free and strained NWs. The strained Pt NWs showed real positive frequency modes, whereas Pd NWs exhibited small imaginary frequencies for the intermediate strain region (≥4%). The strain-free Pt NWs exhibited larger specific heat as compared to Pd NWs, thereby showing excellent electronic thermal and electrical conductivities. The outcome of our study suggests the use of Pt and Pd NWs for different possible applications in spintronic and nanodevices.

## Conflicts of interest

There are no conflicts to declare.

## Acknowledgements

SKG would like to thank the Science and Engineering Research Board (SERB), India for the financial support (Grant no.: YSS/2015/001269).

## References

1 K. K. Korir, G. Cicero and A. Catellani, Piezoelectric properties of zinc oxide nanowires: an *ab initio* study, *Nanotechnology*, 2013, **24**, 475401.
2 Fatima, I. Can Oguz, D. Çakır, S. Hossain, R. Mohottige, O. Gulseren and N. Oncel, On the structural and electronic

properties of Ir-silicide nanowires on Si(001) surface, *J. Appl. Phys.*, 2016, **120**, 095303.
3 S. K. Ray, A. K. Katiyar and A. K. Raychaudhuri, One-dimensional Si/Ge nanowires and their heterostructures for multifunctional applications—a review, *Nanotechnology*, 2017, **28**, 092001.
4 A. Smogunov, A. Dal Corso, A. Delin, R. Weht and E. Tosatti, Colossal magnetic anisotropy of monatomic free and deposited platinum nanowires, *Nat. Nanotechnol.*, 2008, **3**, 22–25.
5 R. Agrawal, J. T. Paci and H. D. Espinosa, Large-Scale Density Functional Theory Investigation of Failure Modes in ZnO Nanowires, *Nano Lett.*, 2010, **10**, 3432–3438.
6 R. H. M. Smit, C. Untiedt, A. I. Yanson and J. M. van Ruitenbeek, Common Origin for Surface Reconstruction and the Formation of Chains of Metal Atoms, *Phys. Rev. Lett.*, 2001, **87**, 266102.
7 S. R. Bahn and K. W. Jacobsen, Chain Formation of Metal Atoms, *Phys. Rev. Lett.*, 2001, **87**, 266101.
8 I. J. T. Jensen, A. G. Ulyashin and O. M. Løvvik, Direct-to-indirect bandgap transitions in ⟨110⟩ silicon nanowires, *J. Appl. Phys.*, 2016, **119**, 015702.
9 S. Kansara, S. K. Gupta, Y. Sonvane and I. Lukačević, Modeling of diameter-dependent Fe and Co ultrathin nanowires from first-principles calculations, *Phys. Chem. Chem. Phys.*, 2017, **19**, 15412–15423.
10 E. Tosatti, Nanowire formation at metal–metal contacts, *Solid State Commun.*, 2005, **135**, 610–617.
11 J. Moreland and J. W. Ekin, Electron tunneling experiments using Nb–Sn "break" junctions, *J. Appl. Phys.*, 1985, **58**, 3888–3895.
12 H. Ohnishi, Y. Kondo and K. Takayanagi, Quantized conductance through individual rows of suspended gold atoms, *Nature*, 1998, **395**, 780–783.
13 E. Li, G. Wu, Z. Cui, D. Ma, W. Shi and X. Wang, Enhancing the field emission properties of Se-doped GaN nanowires, *Nanotechnology*, 2016, **27**, 265707.
14 V. Rodrigues and D. Ugarte, Real-time imaging of atomistic process in one-atom-thick metal junctions, *Phys. Rev. B: Condens. Matter Mater. Phys.*, 2001, **63**, 073405.
15 T. Kizuka, Atomic configuration and mechanical and electrical properties of stable gold wires of single-atom width, *Phys. Rev. B: Condens. Matter Mater. Phys.*, 2008, **77**, 155401.
16 N. Agraït, A. L. Yeyati and J. M. van Ruitenbeek, Quantum properties of atomic-sized conductors, *Phys. Rep.*, 2003, **377**, 81–279.
17 V. Rodrigues, J. Bettini, P. C. Silva and D. Ugarte, Evidence for Spontaneous Spin-Polarized Transport in Magnetic Nanowires, *Phys. Rev. Lett.*, 2003, **91**, 096801.
18 T. H. Yu and C. Ratsch, Computational study of ridge states in GaAs nanopillars, *J. Appl. Phys.*, 2015, **118**, 055703.
19 A. Smogunov, A. Dal Corso and E. Tosatti, Magnetic phenomena, spin-orbit effects, and Landauer conductance in Pt nanowire contacts: density-functional theory calculations, *Phys. Rev. B: Condens. Matter Mater. Phys.*, 2008, **78**, 014423.
20 P. Gambardella, A. Dallmeyer, K. Maiti, M. C. Malagoli, W. Eberhardt, K. Kern and C. Carbone, Ferromagnetism in one-dimensional monatomic metal chains, *Nature*, 2002, **416**, 301–304.
21 G. Rado, *Magnetism*, Elsevier, 2012.
22 P. Gambardella, S. Rusponi, M. Veronese, S. S. Dhesi, C. Grazioli, A. Dallmeyer, I. Cabria, R. Zeller, P. H. Dederichs, K. Kern, C. Carbone and H. Brune, Giant Magnetic Anisotropy of Single Cobalt Atoms and Nanoparticles, *Science*, 2003, **300**, 1130–1133.
23 H. D. Chopra and S. Z. Hua, Ballistic magnetoresistance over 3000% in Ni nanocontacts at room temperature, *Phys. Rev. B: Condens. Matter Mater. Phys.*, 2002, **66**, 020403.
24 J. Velev, R. F. Sabirianov, S. S. Jaswal and E. Y. Tsymbal, Ballistic Anisotropic Magnetoresistance, *Phys. Rev. Lett.*, 2005, **94**, 127203.
25 T. Haug, K. Perzlmaier and C. H. Back, In situ magnetoresistance measurements of ferromagnetic nanocontacts in the Lorentz transmission electron microscope, *Phys. Rev. B: Condens. Matter Mater. Phys.*, 2009, **79**, 024414.
26 K. M. Tsysar, D. I. Bazhanov, A. M. Saletsky, O. O. Brovko and V. S. Stepanyuk, Influence of hydrogen impurities on atomic and electronic structure of palladium nanowires and nanocontacts, *Phys. Rev. B: Condens. Matter Mater. Phys.*, 2011, **84**, 085457.
27 H. Huan, L. Chen and X. Ye, Strain Effect on the Electronic and Optical Properties of CdSe Nanowires, *Nanoscale Res. Lett.*, 2017, **12**, 178.
28 Q. Pang, Y. Zhang, J.-M. Zhang and K.-W. Xu, Adsorption of Ge nanowire with 3d transition metals: a density-functional theory study, *Mater. Chem. Phys.*, 2010, **124**, 1113–1120.
29 M. I. Haftel and K. Gall, Density functional theory investigation of surface-stress-induced phase transformations in fcc metal nanowires, *Phys. Rev. B: Condens. Matter Mater. Phys.*, 2006, **74**, 035420.
30 S. K. R. S. Sankaranarayanan, V. R. Bhethanabotla and B. Joseph, Molecular dynamics simulation of temperature and strain rate effects on the elastic properties of bimetallic Pd–Pt nanowires, *Phys. Rev. B: Condens. Matter Mater. Phys.*, 2007, **76**, 134117.
31 K. Jiang, D. Zhao, S. Guo, X. Zhang, X. Zhu, J. Guo, G. Lu and X. Huang, Efficient oxygen reduction catalysis by subnanometer Pt alloy nanowires, *Sci. Adv.*, 2017, **3**, e1601705.
32 H.-W. Liang, X. Cao, F. Zhou, C.-H. Cui, W.-J. Zhang and S.-H. Yu, A Free-Standing Pt-Nanowire Membrane as a Highly Stable Electrocatalyst for the Oxygen Reduction Reaction, *Adv. Mater.*, 2011, **23**, 1467–1471.
33 S. Guo, S. Zhang, D. Su and S. Sun, Seed-Mediated Synthesis of Core/Shell FePtM/FePt (M = Pd, Au) Nanowires and Their Electrocatalysis for Oxygen Reduction Reaction, *J. Am. Chem. Soc.*, 2013, **135**, 13879–13884.
34 Y. Wang, C. Cong, W. Yang, J. Shang, N. Peimyoo, Y. Chen, J. Kang, J. Wang, W. Huang and T. Yu, Strain-induced direct–indirect bandgap transition and phonon modulation in monolayer WS2, *Nano Res.*, 2015, **8**, 2562–2572.
35 N. Lu, H. Guo, L. Wang, X. Wu and X. Cheng Zeng, van der Waals trilayers and superlattices: modification of

electronic structures of $MoS_2$ by intercalation, *Nanoscale*, 2014, **6**, 4566–4571.

36 S. Kansara, S. K. Gupta and Y. Sonvane, Effect of strain engineering on 2D dichalcogenides transition metal: a DFT study, *Comput. Mater. Sci.*, 2018, **141**, 235–242.

37 B. Y. Xia, H. B. Wu, Y. Yan, X. W. (David) Lou and X. Wang, Ultrathin and Ultralong Single-Crystal Platinum Nanowire Assemblies with Highly Stable Electrocatalytic Activity, *J. Am. Chem. Soc.*, 2013, **135**, 9480–9485.

38 H.-W. Yoo, S.-Y. Cho, H.-J. Jeon and H.-T. Jung, Well-Defined and High Resolution Pt Nanowire Arrays for a High Performance Hydrogen Sensor by a Surface Scattering Phenomenon, *Anal. Chem.*, 2015, **87**, 1480–1484.

39 Y. Im, C. Lee, R. P. Vasquez, M. A. Bangar, N. V. Myung, E. J. Menke, R. M. Penner and M. Yun, Investigation of a Single Pd Nanowire for Use as a Hydrogen Sensor, *Small*, 2006, **2**, 356–358.

40 C. Zhang, L. Xu, Y. Yan and J. Chen, Controlled Synthesis of Pt Nanowires with Ordered Large Mesopores for Methanol Oxidation Reaction, *Sci. Rep.*, 2016, **6**, 31440.

41 J.-H. Lee, J.-H. Park and A. Soon, Assessing the influence of van der Waals corrected exchange-correlation functionals on the anisotropic mechanical properties of coinage metals, *Phys. Rev. B: Condens. Matter Mater. Phys.*, 2016, **94**, 024108.

42 N. V. Ilawe, J. A. Zimmerman and B. M. Wong, Breaking Badly: DFT-D2 Gives Sizeable Errors for Tensile Strengths in Palladium-Hydride Solids, *J. Chem. Theory Comput.*, 2015, **11**, 5426–5435.

43 C. Li, T. Winzer, A. Walsh, B. Yan, C. Stampfl and A. Soon, Stacking-dependent energetics and electronic structure of ultrathin polymorphic V2VI3 topological insulator nano-films, *Phys. Rev. B: Condens. Matter Mater. Phys.*, 2014, **90**, 075438.

44 B. Saha and P. K. Bhattacharyya, Adsorption of amino acids on boron and/or nitrogen doped functionalized graphene: a density functional study, *Comput. Theor. Chem.*, 2016, **1086**, 45–51.

45 C. R. C. Rêgo, L. N. Oliveira, P. Tereshchuk and J. L. F. D. Silva, Comparative study of van der Waals corrections to the bulk properties of graphite, *J. Phys.: Condens. Matter*, 2015, **27**, 415502.

46 M. P. Andersson, Density Functional Theory with Modified Dispersion Correction for Metals Applied to Self-Assembled Monolayers of Thiols on Au(111), *J. Comput. Chem.*, 2013, **2013**, DOI: 10.1155/2013/327839.

47 P. Hohenberg and W. Kohn, Inhomogeneous Electron Gas, *Phys. Rev.*, 1964, **136**, B864–B871.

48 P. Giannozzi, S. Baroni, N. Bonini, M. Calandra, R. Car, C. Cavazzoni, D. Ceresoli, G. L. Chiarotti, M. Cococcioni, I. Dabo, A. D. Corso, S. de Gironcoli, S. Fabris, G. Fratesi, R. Gebauer, U. Gerstmann, C. Gougoussis, A. Kokalj, M. Lazzeri, L. Martin-Samos, N. Marzari, F. Mauri, R. Mazzarello, S. Paolini, A. Pasquarello, L. Paulatto, C. Sbraccia, S. Scandolo, G. Sclauzero, A. P. Seitsonen, A. Smogunov, P. Umari and R. M. Wentzcovitch, QUANTUM ESPRESSO: a modular and open-source software project for quantum simulations of materials, *J. Phys.: Condens. Matter*, 2009, **21**, 395502.

49 D. Vanderbilt, Soft self-consistent pseudopotentials in a generalized eigenvalue formalism, *Phys. Rev. B: Condens. Matter Mater. Phys.*, 1990, **41**, 7892–7895.

50 J. P. Perdew, K. Burke and M. Ernzerhof, Generalized Gradient Approximation Made Simple, *Phys. Rev. Lett.*, 1996, **77**, 3865–3868.

51 J. Heyd, G. E. Scuseria and M. Ernzerhof, Hybrid functionals based on a screened Coulomb potential, *J. Chem. Phys.*, 2003, **118**, 8207–8215.

52 S. Kansara, S. K. Gupta, Y. Sonvane, T. Hussain and R. Ahuja, Theoretical Investigation of Metallic Nanolayers For Charge-Storage Applications, *ACS Appl. Energy Mater.*, 2018, **1**, 3428–3433.

53 T. H. K. Barron and G. K. White, *Heat Capacity and Thermal Expansion at Low Temperatures*, Springer Science & Business Media, 2012.

54 G. K. H. Madsen and D. J. Singh, BoltzTraP. A code for calculating band-structure dependent quantities, *Comput. Phys. Commun.*, 2006, **175**, 67–71.

55 J. F. Scott, Applications of Modern Ferroelectrics, *Science*, 2007, **315**, 954–959.

56 J. Lao and D. Moldovan, Surface stress induced structural transformations and pseudoelastic effects in palladium nanowires, *Appl. Phys. Lett.*, 2008, **93**, 093108.

57 F. Jona and P. M. Marcus, Tetragonal states of palladium I. Theory, *Phys. Rev. B: Condens. Matter Mater. Phys.*, 2002, **65**, 155403.

58 X. Z. Ji, Y. Tian and F. Jona, Tetragonal states of palladium II. Experiment, *Phys. Rev. B: Condens. Matter Mater. Phys.*, 2002, **65**, 155404.

59 A. M. Asaduzzaman and M. Springborg, Structural and electronic properties of Au, Pt, and their bimetallic nanowires, *Phys. Rev. B: Condens. Matter Mater. Phys.*, 2005, **72**, 165422.

60 W. Chao, H. Yanglong, K. Jaemin and S. Shouheng, A General Strategy for Synthesizing FePt Nanowires and Nanorods, *Angew. Chem.*, 2007, **119**, 6449–6451.

61 A. Delin and E. Tosatti, Magnetic phenomena in $5d$ transition metal nanowires, *Phys. Rev. B: Condens. Matter Mater. Phys.*, 2003, **68**, 144434.

62 H. Wang, Q. Li, Y. Gao, F. Miao, X.-F. Zhou and X. G. Wan, Strain effects on borophene: ideal strength, negative Possion's ratio and phonon instability, *New J. Phys.*, 2016, **18**, 073016.

63 A.-X. Zhang, J.-T. Liu, S.-D. Guo and H.-C. Li, Strain effects on phonon transport in antimonene investigated using a first-principles study, *Phys. Chem. Chem. Phys.*, 2017, **19**, 14520–14526.

64 X. Teng, W.-Q. Han, W. Ku and M. Hücker, Synthesis of Ultrathin Palladium and Platinum Nanowires and a Study of Their Magnetic Properties, *Angew. Chem.*, 2008, **120**, 2085–2088.

65 C. Untiedt, D. M. T. Dekker, D. Djukic and J. M. van Ruitenbeek, Absence of magnetically induced fractional

quantization in atomic contacts, *Phys. Rev. B: Condens. Matter Mater. Phys.*, 2004, **69**, 081401.

66 E. C. Stoner, Collective electron ferromagnetism II. Energy and specific heat, *Proc. R. Soc. London, Ser. A*, 1939, **169**, 339–371.

67 G. A. Landrum and R. Dronskowski, The Orbital Origins of Magnetism: From Atoms to Molecules to Ferromagnetic Alloys, *Angew. Chem., Int. Ed.*, 2000, **39**, 1560–1585.

68 S. Kokado, Y. Sakuraba and M. Tsunoda, Spin polarization ratios of resistivity and density of states estimated from anisotropic magnetoresistance ratio for nearly half-metallic ferromagnets, *Jpn. J. Appl. Phys.*, 2016, **55**, 108004.

69 P. V. Leksin, A. A. Kamashev, J. Schumann, V. Kataev and J. Thomas, Probing the degree of spin polarization of a ferromagnet with ferromagnet/superconductor proximity effect, 2017, arXiv:1703.08422.

70 A. H. Reshak, Thermoelectric properties of the spin-polarized half-metallic ferromagnetic CsTe and RbSe compounds, *RSC Adv.*, 2016, **6**, 98197–98207.

71 I. Khan and J. Hong, Manipulation of magnetic state in phosphorene layer by non-magnetic impurity doping, *New J. Phys.*, 2015, **17**, 023056.

72 T. Yildirim and S. Ciraci, Titanium-Decorated Carbon Nanotubes as a Potential High-Capacity Hydrogen Storage Medium, *Phys. Rev. Lett.*, 2005, **94**, 175501.

73 H. Luo, Z. Zhu, G. Liu, S. Xu, G. Wu, H. Liu, J. Qu and Y. Li, Prediction of half-metallic properties for the Heusler alloys Mn2CrZ (Z = Al, Ga, Si, Ge, Sb): a first-principles study, *J. Magn. Magn. Mater.*, 2008, **320**, 421–428.

74 T. Thurn-Albrecht, J. Schotter, G. A. Kästle, N. Emley, T. Shibauchi, L. Krusin-Elbaum, K. Guarini, C. T. Black, M. T. Tuominen and T. P. Russell, Ultrahigh-Density Nanowire Arrays Grown in Self-Assembled Diblock Copolymer Templates, *Science*, 2000, **290**, 2126–2129.

75 A. Delin, E. Tosatti and R. Weht, Magnetism in Atomic-Size Palladium Contacts and Nanowires, *Phys. Rev. Lett.*, 2004, **92**, 057201.

76 Y. Mokrousov, G. Bihlmayer, S. Heinze and S. Blügel, Giant Magnetocrystalline Anisotropies of 4d Transition-Metal Monowires, *Phys. Rev. Lett.*, 2006, **96**, 147201.

77 P. Singh, A. Bala, T. Nautiyal and S. Auluck, An insight into evolution of electronic, magnetic, optical, and vibrational properties of ultrathin Pd nanowires, *J. Nanopart. Res.*, 2013, **15**, 1784.

78 A. Delin and E. Tosatti, The electronic structure of 4d transition-metal monatomic wires, *J. Phys.: Condens. Matter*, 2004, **16**, 8061.

79 J. C. Tung and G. Y. Guo, Magnetic moment and magnetic anisotropy of linear and zigzag 4d and 5d transition metal nanowires: first-principles calculations, *Phys. Rev. B: Condens. Matter Mater. Phys.*, 2010, **81**, 094422.

80 P. K. Sahota, R. Skomski, A. Enders, D. J. Sellmyer and A. Kashyap, Anisotropy of zigzag chains of palladium, *J. Appl. Phys.*, 2011, **109**, 07E322.

81 R. P. Bhatta, S. Annamalai, R. K. Mohr, M. Brandys, I. L. Pegg and B. Dutta, High temperature thermal conductivity of platinum microwire by 3ω method, *Rev. Sci. Instrum.*, 2010, **81**, 114904.

82 B. Y. Terada, K. Ohkubo and T. Mohri, Thermal Conductivities of Platinum Alloys at High Temperatures, *Platinum Met. Rev.*, 2005, **49**, 21–26.

83 X. Zhang, H. Xie, M. Fujii, H. Ago, K. Takahashi, T. Ikuta, H. Abe and T. Shimizu, Thermal and electrical conductivity of a suspended platinum nanofilm, *Appl. Phys. Lett.*, 2005, **86**, 171912.

84 Z.-L. Liu, J.-H. Yang, L.-C. Cai, F.-Q. Jing and D. Alfè, Structural and thermodynamic properties of compressed palladium: *ab initio* and molecular dynamics study, *Phys. Rev. B: Condens. Matter Mater. Phys.*, 2011, **83**, 144113.

85 V. E. Zinovyev, *Metals at high temperatures: standard handbook of properties*, Hemisphere Publ., 1990.

86 B. V. Vlasov, S. G. Taluts, V. E. Zinov'ev, N. A. Korenovskii and V. Polyakova, Kinetic properties of iridium, rhodium, palladium, and platinum in solid and liquid states, *Phys. Met. Metallogr.*, 1992, **74**, 371–377.

87 G. Y. Guo and G. Y. Guo, *J. Appl. Phys.*, 2009, **105**, 07C701 (*J Appl. Phys.*, 2009, **105**, 07C701).

88 G. Hegde, M. Povolotskyi, T. Kubis, J. Charles and G. Klimeck, An environment-dependent semi-empirical tight binding model suitable for electron transport in bulk metals, metal alloys, metallic interfaces, and metallic nanostructures. II. Application-Effect of quantum confinement and homogeneous strain on Cu conductance, *J. Appl. Phys.*, 2014, **115**, 123704.